



Universidade de São Paulo

Biblioteca Digital da Produção Intelectual - BDPI

Departamento de Física e Ciência Interdisciplinar - IFSC/FCI

Artigos e Materiais de Revistas Científicas - IFSC/FCI

2011-06

Effect of "¹⁶O IND. 2' POT. +', "¹H IND. 2' POT. +' + "¹⁶O IND. 2' POT. +', and "¹⁴N IND. 2' POT.+' + "¹⁶O IND. 2' POT. +' ion-beam irradiation on the field emission properties of carbon nanotubes

Journal of Applied Physics, College Park : American Institute of Physics - AIP, v. 109, n. 11, p.
114317-1-114317-7, June 2011
<http://www.producao.usp.br/handle/BDPI/49528>

Downloaded from: Biblioteca Digital da Produção Intelectual - BDPI, Universidade de São Paulo

Effect of O₂⁺, H₂⁺⁺O₂⁺, and N₂⁺⁺O₂⁺ ion-beam irradiation on the field emission properties of carbon nanotubes

J. J. S. Acuña, M. Escobar, S. N. Goyanes, R. J. Candal, A. R. Zanatta, and F. Alvarez

Citation: *Journal of Applied Physics* **109**, 114317 (2011); doi: 10.1063/1.3593269

View online: <http://dx.doi.org/10.1063/1.3593269>

View Table of Contents: <http://scitation.aip.org/content/aip/journal/jap/109/11?ver=pdfcov>

Published by the **AIP Publishing**

Articles you may be interested in

[Carbon nanotubes field emission enhancement using a laser post treatment](#)

J. Vac. Sci. Technol. B **33**, 022203 (2015); 10.1116/1.4913285

[Enhanced field emission from cerium hexaboride coated multiwalled carbon nanotube composite films: A potential material for next generation electron sources](#)

J. Appl. Phys. **115**, 094302 (2014); 10.1063/1.4866990

[Effect of purity, edge length, and growth area on field emission of multi-walled carbon nanotube emitter arrays](#)

J. Appl. Phys. **113**, 204304 (2013); 10.1063/1.4807916

[Effects of deposition and synthesis parameters on size, density, structure, and field emission properties of Pd-catalyzed carbon nanotubes synthesized by thermal chemical vapor deposition](#)

J. Vac. Sci. Technol. B **23**, 793 (2005); 10.1116/1.1880152

[Field Emission from Multiwalled Carbon Nanotubes](#)

AIP Conf. Proc. **633**, 548 (2002); 10.1063/1.1514180




SHIMADZU Excellence in Science **Powerful, Multi-functional UV-Vis-NIR and FTIR Spectrophotometers**

Providing the utmost in sensitivity, accuracy and resolution for applications in materials characterization and nano research

- Photovoltaics
- Polymers
- Thin films
- Paints
- Ceramics
- DNA film structures
- Coatings
- Packaging materials

[Click here to learn more](#)



Effect of O_2^+ , $H_2^+ + O_2^+$, and $N_2^+ + O_2^+$ ion-beam irradiation on the field emission properties of carbon nanotubes

J. J. S. Acuña,¹ M. Escobar,^{2,3} S. N. Goyanes,³ R. J. Candal,^{2,4} A. R. Zanatta,⁵ and F. Alvarez^{1,a)}

¹Instituto de Física “Gleb Wataghin,” UNICAMP, P.O. Box 6165 Campinas, SP, 13083-970, Brazil

²INQUIMAE, FCEyN-UBA-CONICET, Ciudad Universitaria, Pabellón II, Buenos Aires, Argentina

³Depto. Física, FECyN, UBA, Ciudad Universitaria, Pabellón II, Buenos Aires, Argentina

⁴ECyT, 3iA, UNSAM, Campus Migueletes, San Martín, Pcia. Buenos Aires, Argentina

⁵Instituto de Física de São Carlos-USP, P.O. Box 369, São Carlos 13560-250, Brazil

(Received 31 January 2011; accepted 23 April 2011; published online 15 June 2011)

The effect of O_2^+ , $H_2^+ + O_2^+$, and $N_2^+ + O_2^+$ ion-beam irradiation of carbon nanotubes (CNTs) films on the chemical and electronic properties of the material is reported. The CNTs were grown by the chemical vapor deposition technique (CVD) on silicon TiN coated substrates previously decorated with Ni particles. The Ni decoration and TiN coating were successively deposited by ion-beam assisted deposition (IBAD) and afterwards the nanotubes were grown. The whole deposition procedure was performed *in situ* as well as the study of the effect of ion-beam irradiation on the CNTs by x-ray photoelectron spectroscopy (XPS). Raman scattering, field-effect emission gun scanning electron microscopy (FEG-SEM), and field emission (FE) measurements were performed *ex situ*. The experimental data show that: (a) the presence of either H_2^+ or N_2^+ ions in the irradiation beam determines the oxygen concentration remaining in the samples as well as the studied structural characteristics; (b) due to the experimental conditions used in the study, no morphological changes have been observed after irradiation of the CNTs; (c) the FE experiments indicate that the electron emission from the CNTs follows the Fowler-Nordheim model, and it is dependent on the oxygen concentration remaining in the samples; and (d) in association with FE results, the XPS data suggest that the formation of terminal quinone groups decreases the CNTs work function of the material. © 2011 American Institute of Physics. [doi:10.1063/1.3593269]

I. INTRODUCTION

At present, it is recognized that carbon-based materials in the form of nano-tubes, -onions, and -domes have an enormous potential for field-emission devices applications.^{1,2} Carbon nanotubes (CNTs), in particular, are interesting materials with various applications in materials science and electronics.^{3,4} More recently, the incorporation of substitutional atoms in the *graphene* network has been proposed as an alternative route to modify its properties. The inclusion of nitrogen, for example, is expected to change the electronic properties of the material by acting as a donor impurity when incorporated into a graphiticlike structure.^{1,5} However, the effective control over the properties of either N-doped or pure CNT's is critical and requires removal defective structures typically present in these materials.⁶ Previous reports confirm that O^+ ion-beam irradiation of nanotubes preferentially eliminates carbon atoms bonded to highly reactive parts of the material by forming volatile carbon oxide compounds.⁷ Reports relating ion beam purification of nanotubes is not common in the literature.^{1,7} Studies of graphite ion oxygen beam erosion can help to give some clues about the phenomenon involves in the oxygen nanotubes interaction. However, these studies are generally performed by energetic ions (>1 keV) in the attempt to understand the effect of O_2^+

irradiation on graphite in fusion experiments, and consequently, a straight forward comparison with our results is difficult.⁸ Although this limitation, our findings show that the low energy O_2^+ bombardment produces volatiles compounds (CO_2 and CO) as reported with energetic O_2^+ ions probably by eliminating defective C sites.

The etching process takes place because well-organized structures such as fullerenes, nano-domes, -tubes, -onions, and -horns containing graphitic planes are thermodynamically more stable than amorphous (α -)C or other defective structures.^{9–11} We note that, in spite of the extensive use of etching purification process, the mechanisms leading to a better material are not fully understood. Consequently, the study of the microscopic mechanisms involved in the oxygen ion-beam irradiation of nanostructured *graphene*-based materials could improve our understanding as well as lead to further control of their electronic properties.¹² The effect of oxygen etching can be seen, for example, in Fig. 1 where a CNT structure presents flaws and dangling bonds. These defects can react with oxygen species, which are either eliminated or, when remaining attached, act as network terminators.

Based on the above facts, the aim of this paper is to investigate *in situ* the effect of O_2^+ , $H_2^+ + O_2^+$, and $N_2^+ + O_2^+$ ion-beam irradiation on the electronic properties of CNTs deposited by CVD. The analysis of the physical-chemical properties of the nanostructures produced by the ion-beam

^{a)}Electronic mail: alvarez@ifi.unicamp.br.

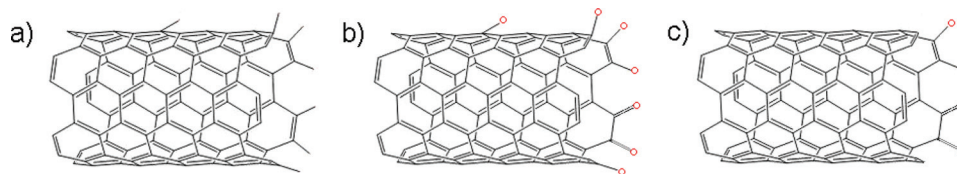


FIG. 1. (Color online) (a) Schematic CNT's showing flaws and dangling bonds. (b) After ion-beam irradiation, oxygen species (open circles) are bonded to these defects. (c) Further sample processing (such as thermal annealing, for example), eliminates very defective regions of the CNT and some oxygen acts as bond terminators (open circles).

irradiation was studied by XPS in a ultrahigh vacuum (UHV) chamber directly attached to the deposition and irradiation chamber, i.e., the samples were analyzed by XPS without atmospheric contamination.¹³ Afterwards, and in order to study the changes in both structural and electronic properties of the material, *ex situ* Raman scattering, electron microscopy, and field emission experiments were performed.

II. EXPERIMENTAL DETAILS

The CNTs are synthesized by CVD using acetylene as a source of carbon on an *in situ* decorated catalyst Ni nanoparticles (NPs) substrate. In fact, the substrate consisted of mirror polished n-type ($\sim 15 \text{ } \Omega/\text{cm}^2$, $<100>$) silicon wafers coated with TiN. The purpose of the TiN film ($\sim 100 \text{ nm}$ thick) is to avoid the formation of nickel silicide and it was grown by ion-beam assisted deposition (IBAD).¹⁴ Briefly, a high-purity titanium target (99.9995%) was sputtered by argon ions (1450 eV, $13 \text{ mA}/\text{cm}^2$) in a nitrogen atmosphere (partial pressure: $4.8 \times 10^{-2} \text{ Pa}$) at 650°C . Afterwards, the Ni NPs were deposited by sputtering a Ni target (99.9995%) which was followed by annealing the sample for 5 min at 650°C . Further details on the Ni island preparation can be found elsewhere.¹⁵ After the catalyst NPs preparation, the temperature of the substrate was raised to 700°C and the CNTs were grown during 5 min by introducing a gaseous mixture of $[\text{H}_2]:[\text{Ar}]:[\text{C}_2\text{H}_2] = 1:10:6 \text{ sccm}$ inside the preparation chamber (kept at 25 Pa). As we shall see below, “carpet like” nanotubes are obtained from this procedure.

Three different series of nanotubes samples were then irradiated *in situ* by O_2^+ , $\text{H}_2^+ + \text{O}_2^+$, $\text{N}_2^+ + \text{O}_2^+$ ion-beams. The chamber partial pressures due to the O_2 , H_2 , and N_2 gases feeding the Kaufman guns was maintained at 1.7×10^{-3} , 1.4×10^{-2} , and $1.9 \times 10^{-2} \text{ Pa}$, respectively. The nominal energy of the ion-beam irradiation was fixed at 30 eV and the current-density beam was $\sim 1.4 \text{ mA}/\text{cm}^2$, i.e., the current measured by the electronic ion gun instrument divided by the area of the Kaufman exit grid of $\sim 3 \text{ cm}$ diameter (Oxford Instrument). Therefore, this grid determines the density of current at the barley exit of the gun. Considering that in the experiment the samples is located $\sim 20 \text{ cm}$ from the gun exit grid, the self ion repulsion spread up the beam to a diameter of $\sim 10\text{--}12 \text{ cm}$ lowering the density of current roughly one order of magnitude, i.e., the beam at the sample is $\sim 0.14 \text{ mA}/\text{cm}^2$. The selection of 30 eV ion energy is a compromise between stability of the ion beam and low energy bombardment of the sample to avoid strong sample damage. Finally, each irradiation procedure is followed by annealing the samples at 400°C for 10 min (in order to remove volatile com-

pounds) and afterwards transferred to the XPS analysis chamber where their structural-chemical characteristics are investigated.

The XPS spectra were taken using the Al $K\alpha$ line ($h\nu = 1486.6 \text{ eV}$) and a VG-CLAMP-2 electron hemispherical analyzer¹⁴ providing a spectral resolution of $\sim 0.85 \text{ eV}$. The atomic composition of the samples was determined by integrating the core-level peaks, properly weighted by the photoemission cross section.¹⁶ The inelastic scattering background contributing to the peaks associated with the electron core-level spectra was subtracted by using Shirley's method.¹⁷ Afterwards, the spectra were adjusted by a standard multiples 50%–50% Gaussian-Lorentzian peaks fitting procedure. The *ex situ*, Raman spectra were obtained in the backscattering geometry by exciting the samples with the 488.0 nm at room-temperature. Scanning electron microscopy (FEG-SEM GEMINI DSM 982) was employed for further characterization of the nanostructures. The SEM images were essentially performed with the main goal to observe possible changes due to the irradiation treatment. Some TEM images (High-Resolution TEM, JEOL JEM-3010 URP) were obtained in few samples with the purpose to determine if the catalyze was on the top or in the bottom of the nanotube, i.e., to discard that some of the observed effects of the field emission experiments were originated in metallic particles. Indeed, the TEM images show that the nickel particles remain in the bottom of the nanotube, i.e., they continue stacked in the substrate after sample growth. It is important to remark that TEM experiments determining the number of nanotubes before and after irradiation as well as their size and type (single wall, multi wall) could bring interesting physical insight on the material properties. At the present we have not systematic TEM images of the samples and more work is necessary before drawing conclusions regarding with the catalyst mechanism of the process. At last comment regarding the catalyst. In accordance with the TEM results, most of the nickel particles remain in the root of the nanotubes. Therefore, the possible formation of metallic compound with O, N, and H will not affect the field emission results.

The field emission characteristics of the samples were studied in a sphere-to-plane electrode configuration, with an anode radii of 1.01 mm, at $\sim 22^\circ\text{C}$, under vacuum conditions ($1.3 \times 10^{-4} \text{ Pa}$). The current versus voltage curves ($I \times V$) are obtained under different electrodes separation and normalized. The $I \times V$ data are well represented by assuming a Fowler-Nordheim emission mechanism. In the case of a parallel plane geometry, if d represents the distance anode-cathode, the density of current J as a function of the electric field $E_0 = V/d$ is given by $J(E_0) = \alpha E_0^2 \exp(-\eta/E_0)$, where, V is

the applied voltage, $\alpha = a\beta^2\phi^{-1}$, and $\eta = b\phi^{3/2}\beta^{-1}$. Here, β and ϕ are the so-called enhancement geometrical factor and work function of the material, respectively. The constants a and b are usually given, in the F-N equation, by $a = e^3/8\pi h$ and $b = 8\pi\sqrt{2m_e}/3eh$, where e and m_e are the charge and electron mass, and h is the Plank's constant. By direct substitution one can obtain $a = 1.54 \times 10^{-6}$ [A eV V⁻²] and $b = 6.83 \times 10^9$ [eV^{-3/2} V m⁻¹].

In the configuration of sphere-to-plane setup electrodes such as those used in this paper, a correction of the F-N equation is necessary and the following expression is obtained for the $I \times V$ relationship:^{18,19}

$$I = 2\pi r V \frac{\alpha}{\eta} \left(\frac{V}{d}\right)^2 \exp\left(\frac{-\eta d}{V}\right). \quad (1)$$

This equation is valid provided that $r \gg d$, where r is the radius of the anode tip. The so-called *linearized F-N form* is written as a function of d/V as:

$$\ln\left(\frac{Id^2}{rV^3}\right) = \ln\left(2\pi\frac{\alpha}{\eta}\right) - \eta\frac{d}{V}, \quad (2)$$

where $-\eta$ is the slope of the straight line represented by Eq. (2). Defining $I(V/d) = A_{eff}J(V/d)$, with r and d geometrical known parameters, by fitting the experimental $I \times V$ data one can obtain the value of η and subsequently the effective emission area given by:

$$A_{eff} = \frac{2\pi r V}{\eta} = \frac{2\pi\beta r V}{b\phi^{3/2}}. \quad (3)$$

As observed in Eq. (3) the effective emission area A_{eff} depends on the applied voltage due to the fact that the anode is curved.¹⁸

It is common to establish the relationship between ϕ and β from the slope of Eq. (2) or the interception of the curve to the ordinate axis. However, previous reports suggest that the former procedure does not always give reliable results.^{20,21}

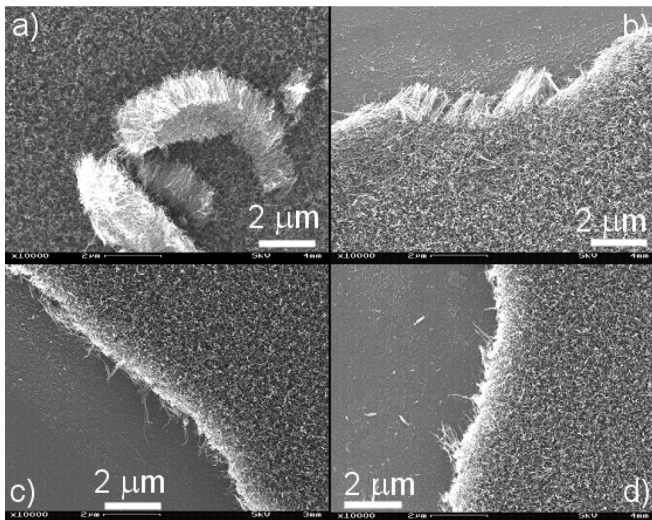


FIG. 2. FEG-SEM images of CNT samples: (a) pristine, and (b) irradiated with (c) O₂⁺, H₂⁺ + O₂⁺, and (d) N₂⁺ + O₂⁺.

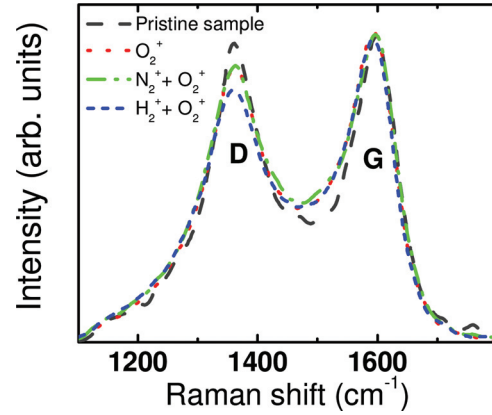


FIG. 3. (Color online) Raman scattering spectra of CNTs irradiated *in situ* with O₂⁺, H₂⁺ + O₂⁺, and N₂⁺ + O₂⁺ ions. D and G stand for the disorder- and graphitelike vibrational modes, respectively.

Therefore, in this paper we used the ordinate at the origin to calculate the relationship $\phi = \phi(\beta)$, where ϕ is given by:

$$\phi = \left(\frac{2\pi a\beta^3}{b\exp(\zeta)}\right)^{2/5}, \quad (4)$$

where $\zeta = \ln(2\pi\alpha/\eta)$ is the intercept defined by Eq. (2).

III. RESULTS

A. Morphological and structural characteristics of the CNTs

Figure 2 presents FEG-SEM micrographs of all the studied samples. Figure 2(a) corresponds to the pristine sample. From this picture (and the deposition time), the growth rate was estimated to be ~ 280 nm/min. The picture shows the carpetlike CNTs in the back plane. The white parts observed in Figure 2(a) correspond to CNTs that were peeled off and moved from a different part of the sample. Figures 2(b), 2(c) and 2(d) correspond to samples irradiated with O₂⁺, H₂⁺ + O₂⁺, and N₂⁺ + O₂⁺ ion-beam, respectively. These pictures show that the main features of the original samples are preserved in spite of the irradiation procedure.

Figure 3 shows the Raman scattering spectra corresponding to samples irradiated with different ion-beam conditions. The spectra show the so-called D-band (~ 1365 cm⁻¹) and G-band (~ 1590 cm⁻¹) that are associated with the presence of structural disorder (mode A_{1g}) and graphite (mode E_{2g}), respectively.^{22,23} The Raman spectra present features that depend on the ion-beam characteristics, which are related to the oxygen incorporation.

TABLE I. Atomic concentration (as obtained from XPS) of the studied CNT samples: before and after irradiation.

| Sample | Carbon (at.%) | Oxygen (at.%) |
|--|---------------|---------------|
| Pristine | 100 | 0 |
| O ₂ ⁺ irradiated | 81 | 19 |
| H ₂ ⁺ + O ₂ ⁺ irradiated | 95 | 5 |
| N ₂ ⁺ + O ₂ ⁺ irradiated | 39 | 61 |

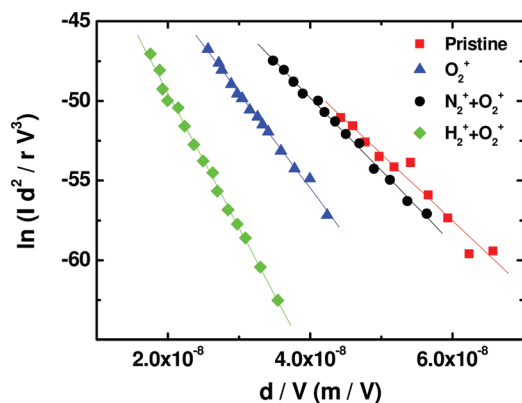


FIG. 4. (Color online) Representation of $\ln(I d^2 / r V^3)$ versus d/V curves, for all studied CNT samples, before and after irradiation.

B. Compositional and structural studies

The carbon and oxygen atomic concentration as obtained from the XPS analysis is shown in Table I. First of all, it must be said that, in the case of the $N_2^+ + O_2^+$ ion-beam the nitrogen concentration remains below 0.5 at.%, i.e., the limit of our detection technique. Also, we have noticed that the presence of H_2^+ in the ion-beam diminishes the amount of oxygen in the material. On the contrary, N_2^+ ions enhanced the oxygen incorporation, which is even higher than that provided by irradiating the samples with pure O_2^+ ions. Considering that the XPS technique probes only the most external surface of the samples (up to ~ 5 nm) one can assume that, most probably, these results correspond to the tips of the nanotubes.

C. Field emission results

Figure 4 presents the $\ln(I d^2 / r V^3)$ versus d/V curves for all of the studied samples. As described in Sec. II this behavior is characteristic of the Flower-Nordheim model, i.e., the transport mechanism is a tunneling emission phenomenon.²⁴ According to the literature, it is common to define the emission threshold field as the applied (macroscopic) electric field (E_0) necessary to produce a fixed current density.

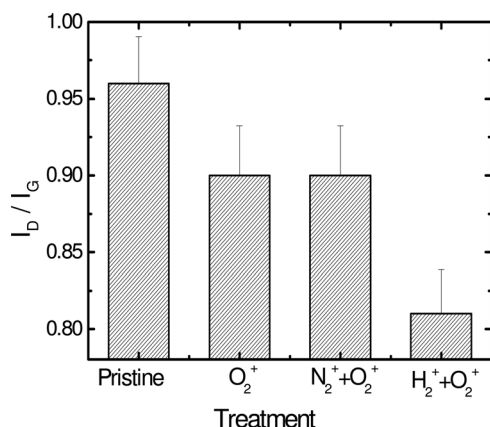


FIG. 5. I_D/I_G peak ratio obtained from the D- and G-bands (Fig. 3) after a two Gaussian fitting procedure of the studied samples.

TABLE II. Summary of the different contributions present in the XPS spectra deconvolution.

| Band | Binding energy (eV) | Chemical bonding |
|-----------------|---------------------|---|
| PC ₁ | 284.4 ± 0.1 | aromatic C—C [1] |
| PC ₂ | 285.3 ± 0.1 | C—C <i>sp</i> ³ type [1,2,13] |
| PC ₃ | 287.5 ± 0.1 | C=O, C—O, and COO [1,2] |
| PC ₄ | 290.1 ± 0.1 | π -plasmons and/or <i>shake-up</i> [15] |
| PO ₁ | 530.3 ± 0.2 | >C=O quinone [38] |
| PO ₂ | 531.7 ± 0.2 | C=O in esters, amides and anhydrides [31] |
| PO ₃ | 533.2 ± 0.2 | —OH [1] |

However, this definition is not adequate considering that the cathode geometry can influence the results.²⁵ As a result, in order to characterize the behavior of the electronic emission, we propose that it is more reliable to calculate the current density J_L obtained when an *arbitrary defined local electric field*, namely, $E_L = 1$ V/nm, is applied. Here $E_L = \beta E_0$, and β , and E_0 were previously defined. Experimental evidence show that E_L is typically a few V/nm, and it is significantly higher than E_0 .^{25,26} Table III shows all the parameters defined in Sec. II and obtained from fitting the Eq. (2) to the experimental results displayed in Fig. 4.

IV. DISCUSSION

A. Morphological and material structural characteristics

As observed from the Raman scattering spectra (Fig. 3), the ion-beam irradiation treatments reduce the contribution of the D-band while the G-band is not modified. In other words, the disorder-associated vibrational modes are the ones mostly affected by the treatment. The effect of the ion-beam characteristic on the decreasing of the I_D/I_G ratio (Fig. 5) suggests an efficient elimination of the more reactive parts of the material—essentially dangling and wrong bonds. Moreover, the Raman spectra present some broadening of the high-frequency side of the G- and D-bands, most probably due to the incorporation of oxygen in the CNTs (Table I).

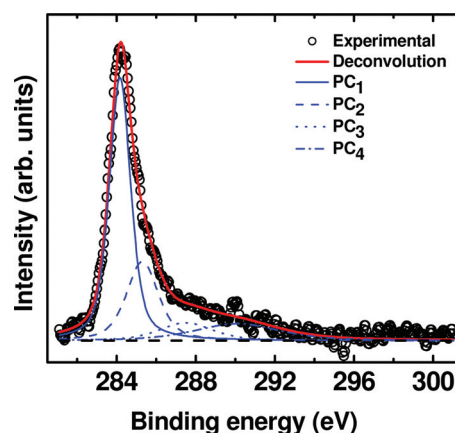


FIG. 6. (Color online) XPS spectrum and PC_i fitting components associated with the C1s core level. The spectrum corresponds to a CNT sample irradiated with $N_2^+ + O_2^+$ ions.

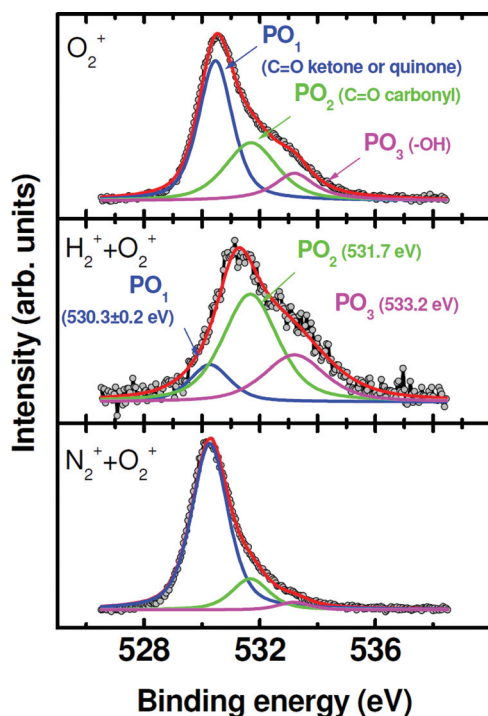


FIG. 7. (Color online) XPS spectra associated to the emission of O1s electrons in a CNT sample after irradiation with O_2^+ , $H_2^+ + O_2^+$, and $N_2^+ + O_2^+$ ions. The circles correspond to the experimental data, and the straight lines to fitting functions (associated to C=O ketone or quinone, C=O carbonyl, and -OH groups).

B. Effect of beam irradiation on the material chemical structure

As mentioned in Sec. III B, the fitting procedure of the structure associated with the band due to C1s electrons yields four bands: PC_i with $i = 1, 2, 3, 4$ (Table II). All the studied samples present C1s XPS spectra similar to the one shown in Fig. 6, which corresponds to the CNT sample irradiated with $N_2^+ + O_2^+$ ions. Here, PC_1 (~ 284.4 eV) is attributed to C—C bonds in graphitic sp^2 configuration; PC_2 (~ 285.3 eV) is related to sp^3 bonded carbon atoms; PC_3 (~ 287.5 eV) is due to carbon in carbonyl (C=O<) and/or quinone groups; and PC_4 (~ 290.1 eV) is associated with the *shake-up* satellites phenomenon, i.e., $\pi \rightarrow \pi^*$ transitions in aromatic systems.¹⁶ Table IV contains the atomic percentage of each of these contributions as well as their corresponding FWHMs.

Table IV roughly shows that independently of the ion-beam composition, the sp^2 bonds forming *graphene* are eroded and, concomitantly, a relative increase of the sp^3 bonds is observed. The increasing number of C=O< and/or quinone complexes are also observed in the irradiated sam-

ples. Finally, the presence of an almost constant contribution of $\pi \rightarrow \pi^*$ transitions (*shake-up*), typical of aromatic systems, suggests that the irradiation does not disrupt the conjugation of double bonds in the *graphene* skeleton.

Figure 7 shows the core levels due to O1s electrons treated after irradiation with O_2^+ , $H_2^+ + O_2^+$, and $N_2^+ + O_2^+$ ions, as indicated in the figure. The fitting of the O1s core level involves three main contributions: PO_1 that is associated with quinone groups; PO_2 that is attributed to carbonyl (C=O<), esters, amides and anhydrides; and PO_3 that corresponds to OH groups (see Table II). For comparison purposes, the relative concentration and FWHM of PO_1 , PO_2 , and PO_3 are shown in Table IV, as a function of the different irradiation details. As can be seen, the data of Table IV suggest that oxygen bond formation strongly depends on the ion-beam characteristics. Moreover, two results are particularly noteworthy: (a) the high contribution of C=O quinoid carbonyl groups (81.2%) in the samples irradiated with the $N_2^+ + O_2^+$ beam (PO_1); and (b) the high contribution of OH groups attached to aromatic rings ($PO_3 \sim 33.8$ at.%) in the CNT samples irradiated with $H_2^+ + O_2^+$ ions.

The material composition and formation of the different structures discussed in connection with the XPS results (Tables I, II, and IV) are a consequence of a complex interplay of chemical reactivity and kinetic of the process influenced by the ion-beam bombardment. The energy of the ions impinging on the surface of the samples is enough to break C-C bonds, leaving dangling bonds to react with activated species such as O_2^+ , N_2^+ , and H_2^+ . The presence of H_2^+ in the ion-beam diminishes the amount of oxygen retained in the material due its affinity with oxygen, explaining the low oxygen concentration retained in the sample. At this point, it is hard to explain why when irradiating with pure O_2^+ ions, the amount of oxygen retained in the samples is smaller than in the case of a $N_2^+ + O_2^+$ irradiation. This result suggests that nitrogen species catalyze the incorporation of oxygen in the material but more work is necessary to improve the understanding of this phenomenon.

The differences in the relative proportion of the functional groups mentioned before can be explained based on their chemical characteristics. The anhydride and esters groups, responsible for the PO_2 signal, are rich in oxygen and can easily leave the carbon skeleton as volatile CO or CO_2 . The simultaneous bombardment of the CNTs with N_2^+ and O_2^+ produces esters or anhydride groups, which are immediately eliminated as CO_2 (or CO), leading to the production of quinoid groups, responsible for the PO_1 signal. On the other hand, the presence of H_2^+ in the $H_2^+ + O_2^+$ ion-beam decreases the concentration of oxygen species probably by the production of H_2O . Besides, the C=O groups can be

TABLE III. Summary of parameters obtained from Fig. 4.

| Sample | d [$\pm 1 \mu\text{m}$] | η [$\pm 1 \text{ V}/\mu\text{m}$] | ζ | A_{eff} [$\pm 10^2 \mu\text{m}^2$] | ϕ ($\beta = 10$) [± 0.5 eV] | J_L ($\beta = 10$) [$\pm 0.1 \text{ mA}/\mu\text{m}^2$] |
|----------------------------|-----------------------------|--|---------|---|---|---|
| Pristine | 19 | 420 | -32.29 | 6600 | 7.4 | 0.9 |
| O_2^+ irradiated | 22 | 593 | -31.69 | 7100 | 5.8 | 1.3 |
| $H_2^+ + O_2^+$ irradiated | 15 | 856 | -32.17 | 3640 | 7.0 | 0.1 |
| $N_2^+ + O_2^+$ irradiated | 17 | 457 | -31.53 | 5440 | 5.4 | 1.5 |

TABLE IV. Atomic concentration (at.%) and FWHM (eV) of the C1s and O1s core levels, as obtained from the XPS analysis. The data correspond to CNT samples irradiated with different ion-beam characteristics. The most probable origin of each PC_i and PO_i contributions are indicated (brackets).

| Sample | PC ₁ (sp ²) | | PC ₂ (sp ³) | | PC ₃ (C=O< and quinoid carbonyl groups) | | PC ₄ (shake-up) | | PO ₁ (quinone groups) | | PO ₂ (carbonyl, esters, amides, etc.) | | PO ₃ (—OH groups) | |
|---|---------------------------------------|--------------|---------------------------------------|--------------|--|--------------|-------------------------------|--------------|--|--------------|--|--------------|---------------------------------|--------------|
| | [C] (at.%) | FWHM (eV) | [C] (at.%) | FWHM (eV) | [C] (at.%) | FWHM (eV) | [C] (at.%) | FWHM (eV) | [O] (at.%) | FWHM (eV) | [O] (at.%) | FWHM (eV) | [O] (at.%) | FWHM (eV) |
| Pristine | 60.5 | 1.2 | 21.2 | 2.0 | 1.6 | 2.0 | 15.5 | 4.9 | — | — | — | — | — | — |
| O ₂ ⁺ | 55.0 | 1.2 | 24.1 | 2.3 | 5.1 | 3.1 | 15.7 | 5.7 | 42.9 | 1.3 | 51.4 | 2.3 | 5.7 | 1.2 |
| H ₂ ⁺ + O ₂ ⁺ | 56.2 | 1.2 | 26.0 | 1.8 | 3.3 | 1.6 | 14.3 | 5.0 | 13.4 | 1.7 | 52.7 | 2.3 | 33.8 | 3.6 |
| N ₂ ⁺ + O ₂ ⁺ | 53.4 | 1.2 | 23.9 | 3.6 | 10.4 | 5.7 | 13.1 | 10.0 | 81.2 | 1.7 | 15.6 | 1.5 | 3.2 | 1.3 |

reduced to Ar-OH (aromatic alcohols) responsible for the PO₃ signal.

C. Electronic properties

The electronic emission parameters obtained by fitting the experimental results shown in Fig. 4 to Eq. (1)–(4) (Sec. II) are displayed in Table III. The β enhancement geometrical factor was assumed 10—a factor generally accepted for CNTs.²⁷ As observed, the largest work function ϕ was achieved in the pristine samples. On the other hand, smaller values were obtained in samples containing more oxygen after the irradiation treatment. Indeed, this finding is consistent with the results reported by other researchers showing that oxygen improves the electronic emission properties of CNTs.^{12,28–32}

The band associated with the O1s core level electrons is located at a relatively low binding energy (530.3 eV), that was recently attributed to the C=O bond of quinoid groups.³³ In particular, within this group there is a functional group, called benzoquinone, which contains two oxygen atoms doubly bonded to carbon in terminal parts of the structure. As discussed before, the bombardment with the N₂⁺ + O₂⁺ ion-beam contributes to the increment in the concentration of quinoid groups at the tips of the CNTs. In contrast, the H₂⁺ + O₂⁺ ion-beam reduces the quinoid concentration. On the other hand, the Raman spectra indicate that the irradiation slightly increases the width of the G-band (Fig. 3), probably due to variations in the angles and length of the sp² type bonds, as well as broken bonds in aromatic rings. We note that the treatment minimizing the structural disorder (Fig. 5) is the one containing H₂⁺ + O₂⁺ ions in the beam. Concomitantly, this treatment leads to less oxygen incorporation in the material (Table I) and to the poorest electron emission properties (Table III). Since for higher J_L electronic emission properties are better, one can conclude that the material irradiated with N₂⁺ + O₂⁺ is improved, i.e., samples containing the highest oxygen concentration present better emission properties. The relative high electronegativity of oxygen can help to understand these findings.⁷ The oxygen atoms are bonded at the tips of the CNTs occupying defects and mostly forming conjugated quinone groups. Therefore, the formation of dipole terminators induced by

oxygen acting on delocalized π -electron may be responsible by decreasing the effective work function of the material.

V. CONCLUSIONS

In this paper we presented a comprehensive study of the effect of O₂⁺, H₂⁺ + O₂⁺, and N₂⁺ + O₂⁺ ion-beam irradiation on the field emission properties of CNTs. The CNTs were grown by the CVD technique using Ni catalyst nanoparticles deposited by ion-beam assisted deposition on silicon substrates. The influence of the ion-beams composition irradiation on the nanotubes structure was studied *in situ* by XPS. Complementary information was gathered by *ex situ* Raman, FEG-SEM. The characteristic parameters associated with field emission properties of the nanotubes were estimated. The work function of the material decreases when oxygen is incorporated in terminator compounds, probably in defects located in aromatic carbon rings present in the CNTs. The treatment with N₂⁺ + O₂⁺ improves the field emission properties due to the formation of benzoquinonic functional group (PO₁ peak) by electronic delocalization (π -orbital) while the treatment with H₂⁺ + O₂⁺ ion-beam increases graphitization. In order to explain these differences we suggest that the heavier N₂⁺ ions induce defects that can bond to oxygen atoms. The relative high electro negativity of the oxygen increases the electronic density at the nano-tubes tips diminishing the work function of the material. The H₂⁺ irradiation, on the contrary, seems to improve the structural order and prevents oxygen incorporation.

Finally, we propose an alternative criterion for evaluating the electron emission of CNT's which, presently, is based on the electric field necessary to obtain an arbitrary electron emission current. Indeed, considering that the cathode-anode shape can influence the field emission results, we suggest that it is more reliable to compare the relative emission goodness of different samples by determining the current density obtained when an arbitrary local electric field is applied.

ACKNOWLEDGMENTS

This work is part of the Ph.D. thesis of JJSA and was partially sponsored by FAPESP (project 05/53926-1). JJSA, ARZ, and FA are CNPq fellows. RJC, SNG and ME are members of CONICET. Also, this work was supported by UBA, Argentina (IP X191); CONICET (PIP 5215 & 5959),

ANPCyT (PICT 10-25834 & 06-10621), Argentine-Brazilian project CAPES – SPU 011/02. The authors are grateful to Mr. C. Piacenti for technical assistance.

- ¹P. Paredez, C. A. Figueroa, L. F. Zagonel, F. R. Reichert, C. T. M. Ribeiro, S. Point, C. Godon, T. M. Minea, and F. Alvarez, *J. Nanosci. and Nanotechnol.* **2**, 188 (2005).
- ²W. A. de Hexer, A. Châtelain, and D. Ugarte, *Science* **270**, 1179 (1995).
- ³A. Bianco, K. Kostarelos, C. D. Partidos, and M. Prato, *Chem. Commun.* **5**, 571 (2005).
- ⁴J.-M. Bonard, J.-P. Salvetat, T. Stockli, W. A. de Heer, L. Forro, and A. Châtelain, *Appl. Phys. Lett.* **73**, 918 (1998).
- ⁵J. J. Li, W. T. Zheng, Z. S. Jin, X. Wang, H. J. Bian, G. R. Gu, Y. N. Zhao, S. H. Meng, X. D. He, and J. C. Han, *J. Vac. Sci. Technol. B* **21**, 2382 (2003).
- ⁶R. Droppa, Jr., C. T. M. Ribeiro, A. R. Zanatta, M. C. dos Santos, and F. Alvarez, *Phys. Rev. B* **68**, 2454 (2004).
- ⁷J. J. S. Acuña, C. A. Figueroa, D. Biggemann, M. U. Kleinke, and F. Alvarez, *J. Appl. Phys.* **103**, 124907 (2008).
- ⁸A. Refke, V. Philipps, and E. Vietzke, *J. Nucl. Mater.* **250**, 13 (1997).
- ⁹H. T. Fang, C. G. Liu, L. Chang, L. Feng, L. Min, and H. M. Cheng, *Chem. Mater.* **16**, 5744 (2004).
- ¹⁰X. Y. Zhu, S. L. Lee, Y. H. Lee, and T. Frauenheim, *Phys. Rev. Lett.* **85**, 2757 (2000).
- ¹¹M. G. Fyta, I. N. Remediakis, and P. C. Kelires, *Phys. Rev. B* **67**, 035423 (2003).
- ¹²Y. Liu, L. Liu, P. Liu, L. Sheng, and S. Fan, *Diam. Relat. Mater.* **13**, 1609 (2004).
- ¹³J. J. S. Acuña, C. A. Figueroa, M. E. H. Maia da Costa, P. Paredez, C. T. M. Ribeiro, and F. Alvarez, *J. Non-Cryst. Solids* **352**, 1314 (2006).
- ¹⁴P. Hammer, N. M. Victoria, and F. Alvarez, *J. Vac. Sci. Technol. A* **16**, 2491 (1998).
- ¹⁵P. Paredez, M. C. Marchi, M. E. H. Maia da Costa, C. A. Figueroa, M. U. Kleinke, C. T. M. Ribeiro, J. C. Sánchez-López, T. C. Rojas, and F. Alvarez, *J. Non-Cryst. Solids* **352**, 1303 (2006).
- ¹⁶D. Briggs and M. P. Seah (Eds.), in *Practical Surface Analysis, Auger and X-Ray Photoelectron Spectroscopy*, 2nd ed, (Wiley, New York, 1993).
- ¹⁷D. A. Shirley, *Phys. Rev. B* **5**, 4709 (1972).
- ¹⁸F. Lacher, C. Wild, D. Behr, and P. Koidl, *Diam. Relat. Mater.* **6**, 1111 (1997).
- ¹⁹M. Boscolo, S. Cialdi, and I. Boscolo, *J. Vac. Sci. Technol. B*, **25**, 1253 (2007).
- ²⁰F. M. Charbonnier, L. A. Southall, and W. A. Mackie, *J. Vac. Sci. Technol. B* **23**, 723 (2005).
- ²¹Y. Gotoh, M. Nagao, M. Matsubara, K. Inoue, H. Tsuji, and J. Ishikawa, *Jpn. J. Appl. Phys.* **35**, L1297 (1996).
- ²²A. C. Ferrari and J. Robertson, *Phys. Rev. B* **61**, 14095 (2000).
- ²³R. O. Dillon and J. A. Woollam, *Phys. Rev. B* **29**, 3482 (1984).
- ²⁴R. H. Fowler and L. Nordheim, *Proc. R. Soc. London A* **119**, 173 (1928).
- ²⁵J. MarcBonard, M. Croci, I. Arfaoui, O. Noury, D. Sarangi, and A. Châtelain, *Diam. Relat. Mater.* **11**, 763 (2002).
- ²⁶R. G. Forbes, C. J. Edgcombe, and U. Valdrè, *Ultramicroscopy* **95**, 57 (2003).
- ²⁷O. Küttel, O. Gröningm, C. E. Nilsson, E. Maillard, L. Diederich, and L. Schlapbach, *Carbon* **37**, 745 (1999).
- ²⁸M. Geis, J. Twichell, J. Macaulay, and K. Okano, *Appl. Phys. Lett.* **67**, 1328 (1995).
- ²⁹Z. Chen, D. denEngelsen, P. K. Bachmann, V. vanElsbergen, I. Koehler, J. Merikhi, and D. U. Wiechert, *Appl. Phys. Lett.* **87**, 243104 (2005).
- ³⁰S. H. Lee, C. H. Lin, J.-M. Chiou, and C. T. Kuo, *Diam. Relat. Mater.* **15**, 854 (2006).
- ³¹S. Y. Han, J. K. Kim, J. L. Lee, and Y. J. Baik, *Appl. Phys. Lett.* **76**, 3624 (2000).
- ³²W. Rochanachirapar, K. Murakami, N. Yamasaki, S. Abo, F. Wakaya, M. Takai, A. Hosono, and S. Okuda, *J. Vac. Sci. Technol. B* **23**, 765 (2005).
- ³³D. Mo and D. Ye, *Surf. Coat. Technol.* **203**, 1154 (2009).